

Cosmic flows on $100 h^{-1}$ Mpc scales: standardized minimum variance bulk flow, shear and octupole moments

Hume A. Feldman,^{1,2,3★} Richard Watkins^{4★} and Michael J. Hudson^{5,6,7★}

¹Department of Physics and Astronomy, University of Kansas, Lawrence, KS 66045, USA

²Department of Physics and Astronomy, University College London, London WC1E 6BT

³Department of Physics, Blackett Laboratory, Imperial College, London SW7 2AZ

⁴Department of Physics, Willamette University, Salem, OR 97301, USA

⁵Department of Physics and Astronomy, University of Waterloo, Waterloo, ON N2L 3G1, Canada

⁶Institut d'Astrophysique de Paris - UMR 7095, CNRS/Université Pierre et Marie Curie, 98bis boulevard Arago, 75014 Paris, France

⁷Perimeter Institute for Theoretical Physics, 31 Caroline St. N., Waterloo, ON N2L 2Y5, Canada

Accepted 2010 May 19. Received 2010 May 17; in original form 2009 November 29

ABSTRACT

The low-order moments, such as the bulk flow and shear, of the large-scale peculiar velocity field are sensitive probes of the matter density fluctuations on very large scales. In practice, however, peculiar velocity surveys are usually sparse and noisy, which can lead to the aliasing of small-scale power into what is meant to be a probe of the largest scales. Previously, we developed an optimal ‘minimum variance’ (MV) weighting scheme, designed to overcome this problem by minimizing the difference between the measured bulk flow (BF) and that which would be measured by an ideal survey. Here we extend this MV analysis to include the shear and octupole moments, which are designed to have almost no correlations between them so that they are virtually orthogonal. We apply this MV analysis to a compilation of all major peculiar velocity surveys, consisting of 4536 measurements. Our estimate of the BF on scales of $\sim 100 h^{-1}$ Mpc has a magnitude of $|v| = 416 \pm 78 \text{ km s}^{-1}$ towards Galactic $l = 282^\circ \pm 11^\circ$ and $b = 6^\circ \pm 6^\circ$. This result is in disagreement with Λ cold dark matter with *Wilkinson Microwave Anisotropy Probe 5* (*WMAP5*) cosmological parameters at a high confidence level, but is in good agreement with our previous MV result without an orthogonality constraint, showing that the shear and octupole moments did not contaminate the previous BF measurement. The shear and octupole moments are consistent with *WMAP5* power spectrum, although the measurement noise is larger for these moments than for the BF. The relatively low shear moments suggest that the sources responsible for the BF are at large distances.

Key words: galaxies: kinematics and dynamics – galaxies: statistics – cosmology: observations – cosmology: theory – distance scale – large-scale structure of the Universe.

1 INTRODUCTION

Large-scale structure formation is assumed to arise from small Gaussian initial fluctuations amplified by gravitational instability (Bardeen et al. 1986; Eisenstein & Hu 1998). This basic framework is strongly supported by the consistency between the cosmic microwave background (CMB) angular power spectra (Dunkley et al. 2009 hereafter *Wilkinson Microwave Anisotropy Probe 5*, *WMAP5*) observed at high redshift and large-scale structure data from gravitational lensing (Fu et al. 2008) and galaxy power spectra (Cole et al. 2005; Eisenstein et al. 2005) and its bispectrum (Feldman et al.

2001; Scoccimarro et al. 2001; Verde et al. 2002), measured at low redshift.

However, on the largest scales, the comparisons are usually between the *matter* density fluctuations measured by the CMB and the fluctuations in *galaxy* number density, and so are susceptible to uncertainties in the relationship between mass and light (biasing). While dark matter (DM) can be observed directly at relatively low redshift via gravitational lensing, at present this technique only just reaches into the linear regime (Fu et al. 2008). The Integrated Sachs–Wolfe (ISW) effect (Sachs & Wolfe 1967) probes the evolution of the DM potential on large scales via a cross-correlation between galaxies and the CMB. Recent ISW compilations suggest a stronger signal than expected (Ho et al. 2008). Perhaps the most promising method for probing the low-redshift DM power spectrum on very large scales ($\lesssim 100 h^{-1}$ Mpc, where h is the Hubble constant

*E-mail: feldman@ku.edu (HAF); rwatkins@willamette.edu (RW); mjhudson@uwaterloo.ca (MJH)

in units of $100 \text{ km s}^{-1} \text{ Mpc}^{-1}$) is via the peculiar velocity field of galaxies and clusters (Strauss & Willick 1995).

Peculiar velocities can be measured statistically through redshift-space distortions of galaxy power spectra (Peacock et al. 2001; Tegmark et al. 2004), or more directly by measuring distances to individual galaxies or clusters. Recent peculiar velocity studies, using various techniques (Pike & Hudson 2005; Park & Park 2006; Sarkar, Feldman & Watkins 2007; Watkins & Feldman 2007; Feldman & Watkins 2008; Watkins, Feldman & Hudson 2009), all suggest that different peculiar velocity surveys, using different distance estimators, are all consistent with sampling the same underlying peculiar velocity field. Moreover, recent peculiar velocity surveys (Masters et al. 2006; Springob et al. 2007, 2009) are deeper, denser and more reliable than ever before. As surveys have gotten larger, our understanding of the distance indicators needed to extract the peculiar velocities, and to control their systematic errors, has also improved. Finally, new analytic techniques have allowed us to better extract information from surveys (Feldman et al. 2003; Radburn-Smith, Lucey & Hudson 2004; Pike & Hudson 2005; Sarkar et al. 2007; Watkins & Feldman 2007; Lavaux et al. 2010).

On small scales ($\lesssim 20 h^{-1} \text{ Mpc}$), peculiar velocities yield results consistent with the *WMAP5*+BAO+SN (baryon acoustic oscillations) Λ cold dark matter (Λ CDM) model value: $(\Omega_m/0.3)^{0.55} \sigma_8 = 0.77 \pm 0.035$ (Komatsu et al. 2009). For example, on these scales, Pike & Hudson (2005) found $(\Omega_m/0.3)^{0.55} \sigma_8 = 0.80 \pm 0.05$, from a comparison of density (galaxy redshift) and peculiar velocity surveys. A statistical analysis of pairwise velocities (Feldman et al. 2003) yields, after correction for non-linearities (Juszkiewicz et al. 2010), a slightly higher result for σ_8 : 1.02 ± 0.18 , but which is still consistent with Komatsu et al. (2009). Abate & Erdođdu (2009) found $(\Omega_m/0.25)^{0.55} \sigma_8 = 0.90_{-0.16}^{+0.22}$ from a correlation function analysis of the Spiral Field I-band (SFI++) over a range of scales $\gtrsim 25 h^{-1} \text{ Mpc}$.

On the very largest scales, however, the agreement is less clear. Previous work has suggested that much of the peculiar velocity of the Local Group (LG) and nearby galaxies is generated by gravitational sources on very large scales, at a level which may be in excess of expectations from the standard Λ CDM model. This evidence comes directly from estimates of the bulk flow (BF) on large scales (Feldman & Watkins 2008; Watkins et al. 2009). It also comes indirectly from galaxy redshift surveys which allow one to estimate how much of the LG's motion is generated locally: the measurement of a low amplitude, misaligned *gravity* dipole from masses within $\gtrsim 60$ – $100 h^{-1} \text{ Mpc}$ then requires that a large component of the LG's motion is generated externally, on larger scales (Pike & Hudson 2005; Lavaux et al. 2010).

Many previous studies of peculiar velocity data have been based on MLE analysis of the entire velocity field (Zaroubi et al. 2001; Abate & Erdođdu 2009). While such studies have the advantage that they use all of the information present, there are disadvantages that arise because all scales are analysed simultaneously. In particular, they are sensitive to treatment of quasi- and non-linear regimes, and to the details of the assumed peculiar velocity errors. Moreover, such studies typically assume a given power spectrum shape a priori. In this work, we isolate the largest scales.

In a recent paper (Watkins et al. 2009, hereafter Paper I), we developed the ‘minimum variance’ (MV) moments that were designed to estimate the BF on a particular scale with minimal sensitivity to small-scale power. Paper I also showed that the BFs from independent peculiar velocity surveys were consistent with each other. In this paper, we extend the formalism to include the next higher elements in the expansion, namely the shear and octupole moments.

These higher order moments contain information about the power spectrum on scales that are large, but not as large as that probed by the BF. The primary goal of this paper is to assess whether these moments, like the BF, have higher amplitude than expected in Λ CDM. Moreover, they also allow us to extract cosmographical information: for example, Lilje, Yahil & Jones (1986) first used the existence of a BF and a shear in the very nearby Universe to determine the approximate distance to the Great Attractor.

It is important to note that in our analysis, since we are fitting to moments of an idealized survey, our model does not change with additional moments, that is, we are estimating individual moments rather than fit a model. In principle, then, our estimates of BF from Paper I should not change in the analysis presented here. However, in practice, our use of an orthogonality constraint as described in Section 2 below will lead to small changes in our BF estimates as we include higher moments.

In Section 2, we introduce the MV weights and the 19 MV moments for the BF, shear and octupole. In Section 3, we discuss the peculiar velocity catalogues analysed here. In Section 4, we present the moment amplitudes and compare these with expectations from cosmological models. We discuss our results in Section 5 and conclude in Section 6.

2 MOMENTS OF THE VELOCITY FIELD

While large-scale flows are still in the linear regime, the statistics of individual galaxy or cluster peculiar velocities S_i are not well described by linear theory due to the existence of non-linear flows on small scales. This problem may be solved by decomposing the velocity field into components, each of which reflects motions on a particular range of scales. Since the statistics of moments associated with large-scale motions can be treated using linear theory, the amplitudes of these moments can be used to put direct constraints on cosmological parameters.

The most commonly used decomposition of the velocity field is a Taylor series expansion (Kaiser 1988; Jaffe & Kaiser 1995), where the components of the velocity field are written as

$$v_i(\mathbf{r}) = U_i + U_{ij}r_j + U_{ijk}r_jr_k + \dots \quad (1)$$

The three zeroth-order constants, U_i , are the components of the oft-discussed ‘BF’. The first-order ‘shear’ tensor, U_{ij} , is symmetric if the velocity field is assumed to be curl-free, as it must be if motions are caused by gravitational instability. Thus the condition that $U_{ij} = U_{ji}$ gives six independent shear components. The second-order tensor, U_{ijk} , which we will call the ‘octupole’ tensor, must also be symmetric for the same reason, so that there are 10 independent octupole components, giving a total of 19 independent components for a second-order expansion.

This expansion is used to decompose the velocity field in a particular volume, typically that occupied by the galaxies in a peculiar velocity survey. Under these circumstances, the BF moments probe scales larger than the diameter of the volume, with each subsequent order probing smaller and smaller scales. However, peculiar velocity surveys typically have complicated geometries, so that moment amplitudes are not comparable between surveys (see Watkins et al. 2009; Sarkar et al. 2007). Indeed, even the interpretation of these moments can be difficult due not only to the complicated distribution of survey objects but also to the varying measurement errors associated with each object.

Interpretation of peculiar velocity data would be much more straightforward if the data were close to an ‘ideal survey’: an infinitely large spherically symmetric survey with no measurement

errors and with a Gaussian radial distribution function $f(r) \propto e^{-r^2/2R_l^2}$, where the parameter R_l designates the depth of the survey. The velocity moments obtained in this way correspond to a known scale, are straightforward to interpret, and are comparable between surveys. While we do not have such ideal surveys, we have some flexibility to force our actual surveys to match such an ideal survey as closely as possible. This flexibility is in the form of a weight for each peculiar velocity datum, which we are free to adjust in an optimal way.

Note that this approach of adjusting the weights to match a given ‘ideal’ geometry is very different from the standard maximum likelihood (MLE) weights, which minimize the measurement error but do not account for the geometry of the survey.

Before we discuss the estimation of the velocity moments using velocity surveys, we must address a problem with the Taylor expansion that arises at second order and beyond. While the zeroth- and first-order moments are orthogonal, there is significant overlap between the BF and the octupole moments. In particular, a pure octupole flow in a given volume V , $v_i = U_{ijk}r_jr_k$, contains a net BF in that volume given by $\int_V U_{ijk}r_jr_k d^3r$. This leads to a strong correlation between the BF and octupole moments.

We can solve this problem by modifying the definition of the octupole moments. We rewrite our expansion of the velocity field in a volume V as

$$v_i(\mathbf{r}) = U_i + U_{ij}r_j + U_{ijk}(r_jr_k - \Lambda_{jk}) + \dots \quad (2)$$

where the constants Λ_{jk} are given by

$$\Lambda_{jk} = \int_V r_jr_k d^3r. \quad (3)$$

For a spherically symmetric volume, as we use here, only the diagonal elements Λ_{11} , Λ_{22} and Λ_{33} are non-zero. When the octupole moments are defined in this way, the 19 moments to second order are orthogonal and have no overlap. A similar procedure can be carried out to remove overlap between the third-order moments and the shear; however, current surveys are not sensitive to higher moments than the octupole and thus in this paper we will focus on the second-order expansion only.

Now that we have defined the velocity moments we are interested in, we turn to how these moments can be estimated using peculiar velocity data. First, it is only possible to measure the line-of-sight peculiar velocity $s = \mathbf{v} \cdot \hat{\mathbf{r}}$. Our expansion for the peculiar velocity field thus translates into an expansion for the line-of-sight velocity field $s(\mathbf{r})$, which can be written as

$$s(\mathbf{r}) = U_i\hat{r}_i + U_{ij}r\hat{r}_i\hat{r}_j + U_{ijk}(r^2\hat{r}_i\hat{r}_j\hat{r}_k - \Lambda_{jk}\hat{r}_i) + \dots \quad (4)$$

For simplicity, we follow Jaffe & Kaiser (1995) and write the second-order expansion in the form of a 19 component vector of moment amplitudes,

$$s(\mathbf{r}) = \sum_{p=1}^{19} U_p g_p(\mathbf{r}), \quad (5)$$

where U_p are the 19 moment amplitudes given by

$$U_p = \{U_x, U_y, U_z, U_{xx}, U_{yy}, U_{zz}, U_{xy}, U_{yz}, U_{zx}, U_{xxx}, U_{yyy}, U_{zzz}, U_{xxy}, U_{yyz}, U_{zzx}, U_{xyy}, U_{yzz}, U_{zxx}, U_{yzy}\} \quad (6)$$

and the mode functions are given by

$$g_p(\mathbf{r}) = \{\hat{r}_x, \hat{r}_y, \hat{r}_z, r\hat{r}_x^2, r\hat{r}_y^2, r\hat{r}_z^2, 2r\hat{r}_x\hat{r}_y, 2r\hat{r}_y\hat{r}_z, 2r\hat{r}_x\hat{r}_z, r^2\hat{r}_x^3 - \Lambda_{xx}\hat{r}_x, r^2\hat{r}_y^3 - \Lambda_{yy}\hat{r}_y, r^2\hat{r}_z^3 - \Lambda_{zz}\hat{r}_z, 3r^2\hat{r}_x^2\hat{r}_y - \Lambda_{xx}\hat{r}_y, 3r^2\hat{r}_y^2\hat{r}_z - \Lambda_{yy}\hat{r}_z, 3r^2\hat{r}_z^2\hat{r}_x - \Lambda_{zz}\hat{r}_x, 3r^2\hat{r}_x^2\hat{r}_y - \Lambda_{xx}\hat{r}_y, 3r^2\hat{r}_y^2\hat{r}_z - \Lambda_{yy}\hat{r}_z, 3r^2\hat{r}_z^2\hat{r}_x - \Lambda_{zz}\hat{r}_x, 6r^2\hat{r}_x\hat{r}_y\hat{r}_z\} \quad (7)$$

where we have used the fact that only the diagonal elements of Λ_{ij} are non-zero.

We first consider an idealized survey, consisting of positions \mathbf{r}_n and exact line-of-sight velocities s_n for a spherically symmetric distribution of N_o objects with a given distribution function $f(r)$. In this case, the ideal velocity moments U_p are just the projections of the velocities on to the mode functions,

$$U_p = \frac{1}{N_o} \sum_{n=1}^{N_o} g_p(\mathbf{r}_n) s_n. \quad (8)$$

Thus the moment amplitudes take the form of linear combinations of the velocities $\sum_n w'_{p,n} s_n$ with the numerical values of the MV weights given by

$$w'_{p,n} = g_p(\mathbf{r}_n) / N_o. \quad (9)$$

We note here that equation (8) applies only for moments that have no overlap, as is true for the moments defined in equation (4). The expression for moment amplitudes when overlapping moments are used is somewhat more complicated.

An actual peculiar velocity survey consists of N objects with positions \mathbf{r}_n and measured line-of-sight velocities S_n with uncertainties σ_n . The measured velocities are assumed to have the form $S_n = s_n + \delta_n$, where δ_n is drawn from a Gaussian distribution of variance $\sigma_n^2 + \sigma_*^2$. Here σ_* is the velocity noise, which accounts for small-scale motions not included in the measured moment. In the peculiar velocity literature, the approach often taken is one where one fits a flow model (whether parametric flow model, e.g. an expansion over many components, or using a ‘template’ based on e.g. the gravity of a galaxy density field). In such cases, it is important that the flow model is complete on all scales and that the noise estimates and χ^2 values are reasonable. That is not the approach taken here: instead we are estimating large-scale moments, which are expected to be close to orthogonal. Hence, the value of σ_* affects our moments only very weakly: it modifies the measurement noise and hence the weights. While it has the strongest effect on nearby galaxies for which the velocity errors are smallest, these same galaxies are strongly downweighted by our $R_l = 50 h^{-1}$ Mpc MV weighting scheme. Consequently, changing the value of σ_* does not alter any of our moments significantly.

Given an idealized survey with velocity moments U_p , we wish to determine the weights $w_{p,n}$ such that the linear combinations

$$u_p = \sum_{n=1}^N w_{p,n} S_n \quad (10)$$

give the best possible estimates of the U_p . Following our previous work (Paper I), we calculate the weights by minimizing the average variance $\langle (U_p - u_p)^2 \rangle$. When considering only the BF moments in Paper I, we included additional constraints that ensured that the estimators would give the correct amplitude for a pure BF velocity field. Here we implement a more general set of constraints that is applicable to higher order velocity moments.

Suppose that the flow field consisted only of BF, shear and octupole moments, so that the line-of-sight velocities at positions \mathbf{r}_n took the form $s_n = \sum_p U_p g_p(\mathbf{r}_n)$. In order for the estimators to give the correct amplitudes for the velocity moments on average for this flow field, i.e. $\langle u_p \rangle = U_p$, we require that

$$\sum_n w_{p,n} g_q(\mathbf{r}_n) = \delta_{pq}. \quad (11)$$

This set of constraints can be implemented by using Lagrange multipliers. Thus we seek to minimize the quantity

$$\langle (U_p - u_p)^2 \rangle + \sum_q \lambda_{pq} \left[\sum_n w_{p,n} g_q(\mathbf{r}_n) - \delta_{pq} \right]. \quad (12)$$

Expanding out the first term, plugging in the expression for u_p from equation (10), we can write this expression in terms of the weights $w_{p,n}$,

$$\begin{aligned} \langle U_p^2 \rangle - \sum_n 2w_{p,n} \langle S_n U_p \rangle + \sum_{n,m} w_{p,n} w_{p,m} \langle S_n S_m \rangle \\ + \sum_q \lambda_{pq} \left[\sum_n w_{p,n} g_q(\mathbf{r}_n) - \delta_{pq} \right]. \end{aligned} \quad (13)$$

To find the weights that minimize this expression, we take the derivative with respect to $w_{p,n}$, set it equal to zero:

$$-2 \langle S_n U_p \rangle + 2 \sum_m w_{p,m} \langle S_n S_m \rangle + \sum_q \lambda_{pq} g_q(\mathbf{r}_n) = 0 \quad (14)$$

and solve for the weights,

$$w_{p,n} = \sum_m G_{nm}^{-1} \left[\langle S_m U_p \rangle - \frac{1}{2} \sum_q \lambda_{pq} g_q(\mathbf{r}_n) \right], \quad (15)$$

where G is the covariance matrix of the individual measured velocities, $G_{nm} \equiv \langle S_n S_m \rangle$. The values of the Lagrange multipliers can be found by plugging equation (15) into equation (11) and solving for λ_{pq} ,

$$\lambda_{pq} = \sum_l \left[M_{pl}^{-1} \left(\sum_{m,n} G_{nm}^{-1} \langle S_m U_l \rangle g_q(\mathbf{r}_n) - \delta_{lq} \right) \right], \quad (16)$$

where the matrix M is given by

$$M_{pq} = \frac{1}{2} \sum_{n,m} G_{nm}^{-1} g_p(\mathbf{r}_n) g_q(\mathbf{r}_m). \quad (17)$$

Equation (15) gives us a formula for calculating the MV weights in terms of the covariance matrix $G_{nm} = \langle S_n S_m \rangle$ and the correlation $\langle S_m U_p \rangle$, both of which can be calculated given a power spectrum model. Using the fact that $S_n = s_n + \delta_n$ as described above and that s_n and δ_n are independent, we can write the covariance matrix as

$$\begin{aligned} G_{mn} &= \langle s_m s_n \rangle + \delta_{mn} (\sigma_*^2 + \sigma_n^2) \\ &= \langle \hat{\mathbf{r}}_m \cdot \mathbf{v}(\mathbf{r}_m) \hat{\mathbf{r}}_n \cdot \mathbf{v}(\mathbf{r}_n) \rangle + \delta_{mn} (\sigma_*^2 + \sigma_n^2). \end{aligned} \quad (18)$$

In linear theory, the first term can be expressed as an integral over the density power spectrum $P(k)$,

$$\langle \hat{\mathbf{r}}_m \cdot \mathbf{v}(\mathbf{r}_m) \hat{\mathbf{r}}_n \cdot \mathbf{v}(\mathbf{r}_n) \rangle = \frac{\Omega_m^{1.1}}{2\pi^2} \int dk P(k) f_{mn}(k), \quad (19)$$

where the function $f_{mn}(k)$ is the angle-averaged window function (WF)

$$\begin{aligned} f_{mn}(k) &= \int \frac{d^2 \hat{\mathbf{k}}}{4\pi} \left(\hat{\mathbf{r}}_m \cdot \hat{\mathbf{k}} \right) \left(\hat{\mathbf{r}}_n \cdot \hat{\mathbf{k}} \right) \\ &\quad \times \exp \left[i \mathbf{k} \cdot (\mathbf{r}_m - \mathbf{r}_n) \right]. \end{aligned} \quad (20)$$

The correlation $\langle S_m U_p \rangle$ is calculated in a similar way. We generate an ideal survey by selecting N_o random positions $\mathbf{r}'_{n'}$ with the desired radial distribution function. We can then write

$$\langle S_m U_p \rangle = \sum_{n'} w'_{pn'} \langle s_m s_{n'} \rangle, \quad (21)$$

where the weights $w'_{pn'}$ are the ideal weights given in equation (9) and we have assumed that measurement errors are uncorrelated with velocities. The correlation $\langle s_m s_{n'} \rangle$ can be calculated in the same manner as the elements of the covariance matrix G (equation 18).

Once we have calculated the weights for the MV moments, it is straightforward to calculate their correlation matrix,

$$\begin{aligned} R_{pq} &= \langle u_p u_q \rangle = \sum_{mn} w_{pm} w_{qn} \langle S_m S_n \rangle \\ &= \sum_{mn} w_{pm} w_{qn} G_{mn}. \end{aligned} \quad (22)$$

The moment covariance matrix can be separated into two parts

$$R_{pq} = R_{pq}^{(v)} + R_{pq}^{(\epsilon)}, \quad (23)$$

corresponding to the two terms in G_{nm} . The second term represents the noise in the measurement of the moment

$$R_{pq}^{(\epsilon)} = \sum_n w_{pn} w_{qn} (\sigma_n^2 + \sigma_*^2). \quad (24)$$

The first term is due to actual motions of the objects in the survey and can be written as an integral over the density fluctuation power spectrum,

$$R_{pq}^{(v)} = \frac{\Omega_m^{1.1}}{2\pi^2} \int dk P(k) \mathcal{W}_{pq}^2(k), \quad (25)$$

where the angle-averaged tensor WF is

$$\mathcal{W}_{pq}^2 = \sum_{m,n} w_{pm} w_{qn} f_{mn}(k). \quad (26)$$

The diagonal elements \mathcal{W}_{pp}^2 are the WFs for the individual moments u_p . The WF for a particular moment indicates which scales that moment probes. It can also be compared to the WF for the ideal moment to see the particular scales on which the moments differ.

In summary, our MV method is a two-step process: for each moment, determine the optimal MV weights via equation (15), then use these weights to measure the moments themselves (equation 10). The weights depend only weakly on the power spectra and nuisance parameters (σ_*), so the measured moments are robust. For a given moment, we can also calculate its measurement variance (the diagonal elements of $R_{pq}^{(\epsilon)}$) and the cosmic variance (via $R_{pq}^{(v)}$). Note that the cosmic variance is for the actual MV weights and not the ideal ones. The two variances then allow us to compare the actual moment amplitudes with expectations from cosmological models.

3 DATA

As in Paper I, the peculiar velocity data used here compiles all of the major peculiar velocity surveys published to date, with the exception of the survey of Lauer & Postman (1994), which was found in Paper I to be inconsistent with other data sets. As in Paper I, we have removed outliers by using the predictions of the *IRAS*-PSCz (Point Source Catalogue Redshift) density field (for more details see Paper I; Hudson et al. 2004; Neill, Hudson & Conley 2007). Each individual survey has a characteristic MLE depth, defined as $\sum r_n w_n / \sum w_n$, where the MLE weights are $w_n = 1/(\sigma_n^2 + \sigma_*^2)$.

This compilation, which we label ‘COMPOSITE’, consists of a number of surveys, the largest of which is the SFI++ peculiar

velocity survey of spirals in the field and in groups (Masters et al. 2006; Springob et al. 2007, 2009). Here we use the data from the corrected data set (Springob et al. 2009) rather than from the erroneous one (Springob et al. 2007). After rejecting about 1 per cent of the data, the sample consists of 2720 Tully–Fisher (TF) galaxies and 736 groups to make 3456 data points with characteristic depth of $35 h^{-1}$ Mpc. The SFI++ sample is all-sky, except for the Galactic plane ($|b| \lesssim 15$). As in Paper I, we find that all of the surveys we studied are consistent with each other, with the possible exception of the Lauer & Postman (LP; 1994) brightest cluster galaxy (BCG) survey. The MV-weighted BF of LP disagrees with that of the COMPOSITE catalogue on all scales. The level of disagreement on the larger scales corresponds to 99 per cent confidence level (CL). There are independent reasons to question the LP results: Hudson et al. (2004) compared, cluster by cluster, the distance to the BCG derived by LP to that derived from the fundamental plane (FP) for other cluster members, and found that in a few cases, these distances differed significantly, in the sense that the LP BCG distance was too large (i.e. the BCG was fainter than expected). They found that all of the discrepant BCGs for which *Hubble Space Telescope* images were available showed strong evidence for dust. For these reasons, we have chosen to reject LP from the COMPOSITE catalogues.

It is interesting to compare the results from SFI++ with a completely independent peculiar velocity data set of comparable depth and statistical power. The consistency between these two catalogues, which use different data and methods, is an important check on our results. As in Paper I, we define the ‘DEEP’ compilation including 103 Type Ia supernovae (SNIa) (Tonry et al. 2003), 70 SC TF clusters (Giovanelli et al. 1998b; Dale et al. 1999a), 56 SMAC FP clusters (Hudson et al. 1999, 2004), 50 EFAR FP clusters (Colless et al. 2001) and 15 TF clusters (Willick 1999). The DEEP catalogue consists of 294 data points, but because these are clusters or supernovae their peculiar velocity errors are lower per object than for SFI++. The DEEP compilation covers the whole sky outside the Galactic plane and has a characteristic depth of $50 h^{-1}$ Mpc.

In Paper I, we analysed a further compilation, dubbed ‘SHALLOW’ that consisted of the ENEAR (da Costa et al. 2000; Bernardi et al. 2002; Wegner et al. 2003) survey and a surface brightness fluctuations (SBF) survey (Tonry et al. 2001). Because for our purposes this compilation is rather shallow; we do not analyse it separately here, but include it in COMPOSITE.

In Paper I, we showed that all of these subsets (SFI++, DEEP and SHALLOW) are consistent with the same underlying velocity field, given their sparse spatial sampling. The formalism for comparing

surveys with different WFs is given in Paper I (see equation 24 and Table 3).

In summary, the COMPOSITE catalogue covers the whole sky outside the Galactic plane and has a characteristic depth of $34 h^{-1}$ Mpc. It is based on 4536 peculiar velocity measurements, making it the largest peculiar velocity catalogue compiled and studied to date.

4 RESULTS

4.1 Bulk flow, shear and octupole moments

We calculated the MV moments for the BF, shear and octupole components using the methods described in Section 2 above for each of the catalogues described in Section 3. For specificity, we used the Λ CDM power spectrum model of Eisenstein & Hu (1998) with the *WMAP5* central parameters, $\sigma_8 = 0.796$, $h = 0.719$, $\Omega_m = 0.258$ and $n_s = 0.963$ for the amplitude of cosmological density fluctuations, the Hubble constant, the normalized matter density and the spectral index, respectively, and the velocity noise $\sigma_* = 150 \text{ km s}^{-1}$. The exact values of the cosmological parameters, including σ_* , make little difference to the values of the weights.

In principle, our MV weights allow us to match any choice of ‘ideal window’, which here is assumed to have a Gaussian profile, parametrized by R_I . Clearly, the larger, the denser and more geometrically complete the catalogue is and the smaller the velocity errors are, the closer its window functions resemble that of the ideal window. In practice, however, there is a compromise between two competing goals: one is the need to adjust the weights, as best we can, so that the weighted catalogue matches the ideal survey and the other is to keep the noise small by down-weighting objects with the large measurement errors. Although we have investigated a range of scales $R_I \in [10, 60] h^{-1}$ Mpc, in this paper, we will focus on the window with $R_I = 50 h^{-1}$ Mpc. This choice is a compromise between the desire to probe the largest possible scales and the natural characteristic depths of the catalogues ($\sim 35 h^{-1}$ Mpc). The observational noise is minimized for low R_I and becomes too large if $R_I > 50 h^{-1}$ Mpc.

Fig. 1 shows the peculiar velocity data on the sky, both for MLE weights and for MV weights. Notice how the MV weights become larger in regions where the spatial sampling is poorer, such as close to the Galactic plane. The weighted radial distribution galaxies is shown in Fig. 2, where it is compared to the unweighted, MLE and $R_I = 50 h^{-1}$ Mpc ideal distributions. It is clear that the MV distribution closely approximates that of the ideal one.

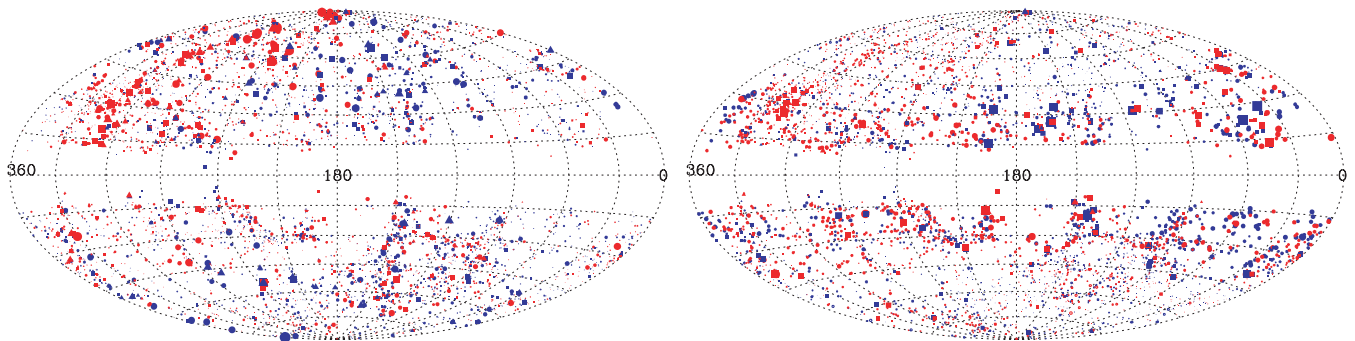


Figure 1. The COMPOSITE peculiar velocity catalogue on the sky (Galactic coordinates). While it is customary in such plots to encode the amplitude of the peculiar velocity by the size of the symbol, in this case symbol area is proportional to the weight. Data from SFI++ are shown by circles, DEEP by squares and SHALLOW by triangles. The left-hand panel shows the MLE weights, whereas the right-hand panel shows the average MV weights.

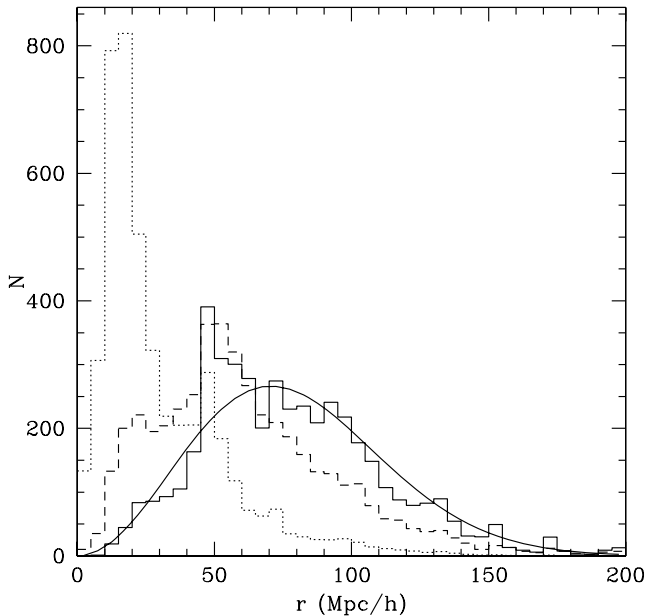


Figure 2. The COMPOSITE peculiar velocity catalogue as a function of depth. The dashed histogram shows the distribution of peculiar velocity measurements. The dotted histogram shows the *weighted* histogram (renormalized to the same area) but using the usual MLE weights. Note that most of the signal is driven by very nearby objects. The solid histogram is also weighted, but using MV weights. The smooth curve shows the expected weighted radial distribution for an ideal survey i.e. $\propto r^2 \exp[-r^2/(2R_I^2)]$. This shows that our MV weighting scheme produces the desired radial distribution.

We compared the WFs (equation 26) of all surveys and composite catalogues to the ideal survey. In Figs 3 and 4 we show both the ideal and survey MV BF, shear and octupole squared tensor WFs (equation 26) for the COMPOSITE survey for $R_I = 50 h^{-1}$ Mpc. The advantage of the MV moments is that they have been designed to be sensitive *only* to a narrow range of scales, and so we will be able to probe these scales without having to worry about the influence of, or aliasing from, smaller scales. The BF moments probes scales much larger than R_I ; the shear responds to R_I scales and larger while the octupole to somewhat smaller scales (see Figs 3 and 4).

When the WFs in Fig. 3 are convolved by the *WMAP5* power spectrum, one finds that, for the BF statistic with $R_I = 50 h^{-1}$ Mpc, the contribution to the integrand in equation 25 peaks at a wavenumber $k \sim 0.01 h \text{ Mpc}^{-1}$, corresponding to wavelengths in excess of $600 h^{-1}$ Mpc. The shear is most sensitive to scales where the BF window is at its minimum, $k \sim 0.025 h \text{ Mpc}^{-1}$ or wavelengths of $250 h^{-1}$ Mpc. It is worth noting that these scales are similar to or larger than the very largest scales probed by Sloan Digital Sky Survey and 2 degree Field Galaxy Redshift Survey (2dFGRS; e.g. Percival et al. 2007). The octupole is sensitive to slightly smaller scales.

Figs 3 and 4 also show that the ideal and survey WFs match well, especially for the lower moments. This is also apparent in Tables 1–3, where we give the values of each moment and the correlation coefficient $\langle \mathbf{u} \cdot \mathbf{U} / |\mathbf{u}| |\mathbf{U}| \rangle$ between the ideal and their MV estimates for each of the moments; a correlation coefficient of unity indicates perfect correlations. We see that the denser the catalogue, the better its match with the ideal moments.

To compare the measured moments with expectations from cosmology, we need to know what moments would be expected. We

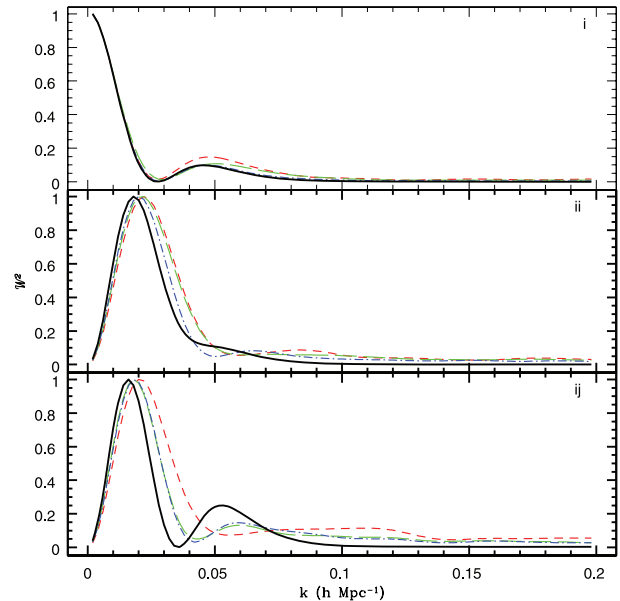


Figure 3. The WFs of the BF and shear moments for $R_I = 50 h^{-1}$ Mpc for the COMPOSITE catalogue. The thick black lines are the ideal WFs for the MV components (since the ideal survey is isotropic, all component are the same), whereas the thin lines are the actual components for the survey. In the top panel are the BF x (short-dash), y (long-dash), z (dot-dashed) components. The middle panel shows the shear xx (short-dash), yy (long-dash), zz (dot-dashed) components, the bottom panel shows the shear xy (short-dash), yz (long-dash) and zx (dot-dashed) components. Note how the WF virtually vanish at large k (small scales). All coordinates are Galactic.

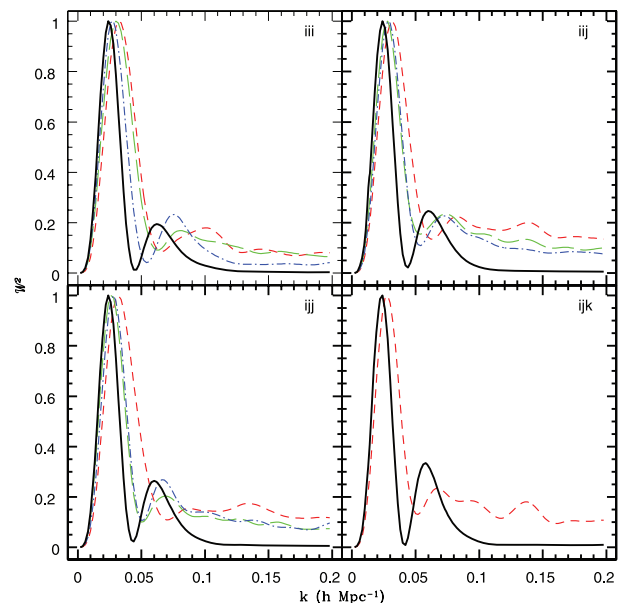


Figure 4. The same as Fig. 3 for the octupole moments. The thick black lines represent the ideal WF. In the top left panel are the xxx (short-dash), yyy (long-dash), zzz (dot-dashed); the top right panel shows the xxy (short-dash), yyz (long-dash), zzx (dot-dashed); the bottom left panel shows the xyy (short-dash), yzz (long-dash) and zxx (dot-dashed); the bottom right panel shows the xyz (short-dash) component of the WF's.

Table 1. The moment's value and its correlation coefficient $\langle uU/|u||U| \rangle$ for each of the catalogues and $R_l = 50 h^{-1} \text{Mpc}$; $N_{\text{MOM}} = 19$. All directions are given in Galactic coordinates. The last column is the expectation value of the moment given *WMAP5* central parameters and the COMPOSITE catalogue WF's as described in the text.

	COMPOSITE		SFI++		DEEP		WMAP CRMS
<i>x</i>	86.5 ± 68.8	0.74	69.0 ± 95.7	0.64	192.7 ± 115.6	0.51	110.6
<i>y</i>	-404.9 ± 61.8	0.77	-473.6 ± 87.2	0.67	-320.7 ± 106.0	0.51	109.0
<i>z</i>	42.8 ± 37.7	0.89	57.7 ± 59.3	0.80	62.0 ± 55.8	0.76	105.3
<i>xx</i>	2.73 ± 1.01	0.69	3.36 ± 1.29	0.62	2.19 ± 1.76	0.47	1.656
<i>yy</i>	1.37 ± 0.98	0.69	3.72 ± 1.27	0.63	-0.19 ± 1.79	0.42	1.547
<i>zz</i>	-0.03 ± 0.68	0.80	2.72 ± 0.96	0.71	-0.72 ± 1.04	0.67	1.462
<i>xy</i>	0.13 ± 0.76	0.51	-0.71 ± 0.98	0.42	0.27 ± 1.29	0.31	0.890
<i>yz</i>	-0.95 ± 0.57	0.63	-1.05 ± 0.78	0.52	-0.71 ± 0.94	0.40	0.749
<i>zx</i>	1.22 ± 0.54	0.66	1.50 ± 0.74	0.56	0.98 ± 0.84	0.47	0.767
<i>xxx</i>	-1.2e-02 ± 2.2e-02	0.38	-9.3e-03 ± 2.9e-02	0.31	1.0e-02 ± 3.6e-02	0.25	1.83e-02
<i>yyy</i>	-2.4e-02 ± 1.7e-02	0.41	-1.9e-02 ± 2.4e-02	0.34	-2.2e-02 ± 2.7e-02	0.24	1.43e-02
<i>zzz</i>	-7.2e-03 ± 1.1e-02	0.61	-3.3e-03 ± 1.6e-02	0.48	-2.5e-03 ± 1.6e-02	0.47	1.28e-02
<i>xyy</i>	-8.2e-03 ± 1.2e-02	0.30	-3.3e-02 ± 1.7e-02	0.23	2.0e-02 ± 1.9e-02	0.20	8.39e-03
<i>yzz</i>	5.8e-04 ± 6.6e-03	0.44	-1.8e-03 ± 1.0e-02	0.33	8.9e-03 ± 9.6e-03	0.30	5.44e-03
<i>zxx</i>	7.3e-03 ± 7.8e-03	0.45	8.7e-03 ± 1.1e-02	0.34	-2.1e-03 ± 1.2e-02	0.34	6.60e-03
<i>xyx</i>	8.3e-03 ± 1.2e-02	0.29	5.7e-03 ± 1.6e-02	0.24	2.2e-02 ± 1.9e-02	0.16	8.24e-03
<i>yyz</i>	6.3e-04 ± 8.3e-03	0.40	7.7e-03 ± 1.2e-02	0.28	-2.5e-03 ± 1.2e-02	0.30	6.35e-03
<i>zzx</i>	1.2e-02 ± 7.6e-03	0.46	-2.5e-03 ± 1.1e-02	0.35	1.6e-02 ± 1.1e-02	0.34	6.86e-03
<i>xyz</i>	6.6e-03 ± 5.5e-03	0.34	9.3e-03 ± 8.2e-03	0.25	4.9e-03 ± 8.2e-03	0.22	3.72e-03

Table 2. The same as Table 1 for $N_{\text{MOM}} = 9$.

	COMPOSITE		SFI++		DEEP		WMAP CRMS
<i>x</i>	101.8 ± 38.4	0.87	65.0 ± 46.9	0.82	127.6 ± 62.9	0.70	110.6
<i>y</i>	-362.2 ± 39.4	0.86	-361.6 ± 47.8	0.81	-326.3 ± 66.1	0.65	109.0
<i>z</i>	40.1 ± 30.9	0.92	76.6 ± 40.3	0.87	49.2 ± 47.8	0.80	105.3
<i>xx</i>	2.89 ± 0.98	0.69	3.94 ± 1.25	0.63	2.39 ± 1.61	0.51	1.656
<i>yy</i>	1.21 ± 0.95	0.69	3.90 ± 1.22	0.64	-0.77 ± 1.68	0.41	1.547
<i>zz</i>	0.10 ± 0.67	0.80	2.76 ± 0.93	0.72	-0.69 ± 1.00	0.68	1.462
<i>xy</i>	0.20 ± 0.74	0.51	-0.76 ± 0.95	0.43	0.22 ± 1.23	0.31	0.890
<i>yz</i>	-1.02 ± 0.55	0.63	-1.11 ± 0.76	0.52	-0.63 ± 0.86	0.41	0.749
<i>zx</i>	1.44 ± 0.53	0.67	1.48 ± 0.72	0.56	1.32 ± 0.80	0.48	0.767

Table 3. The same as Table 1 for $N_{\text{MOM}} = 3$.

	COMPOSITE		SFI++		DEEP		WMAP CRMS
<i>x</i>	97.4 ± 38.3	0.87	71.7 ± 46.4	0.82	120.0 ± 61.2	0.71	110.6
<i>y</i>	-361.9 ± 39.2	0.86	-363.3 ± 46.9	0.82	-333.8 ± 65.4	0.65	109.0
<i>z</i>	41.2 ± 30.7	0.92	73.1 ± 39.8	0.87	44.3 ± 47.1	0.80	105.3

have only a single measurement of each moment (because the flow field is expanded around the origin, i.e. at the location of the LG), but we can calculate what values might have been measured at other locations in a Λ CDM universe (assuming the Copernican principle). For each moment, we can determine its expected mean and variance by calculating ensemble averages over all possible observers. Due to isotropy and homogeneity, the mean must vanish and so it is the variance that is the quantity of interest because it indicates the range of amplitudes for each moment that one would expect. We will call the corresponding standard deviation, the ‘cosmic root mean square’ (CRMS) since it provides an estimate of the expected amplitude of the moment for a survey with the same geometry and weights, but with no measurement noise. In detail, the CRMS is given by the diagonal elements of the covariance matrix $R_{pq}^{(v)}$ (equation 25), which in turn depends on the weights (and hence the measurement noise) and on the power spectrum, but does not include a contribution

from the measurement noise. Tables 1–3 include for comparison the CRMS of each moment around its zero mean, given the spectrum specified by the *WMAP5* central parameters and given the weights as determined above.

Turning to the values of the moments themselves, Tables 1–3 show that there is a remarkable agreement, within the errors, among all catalogues and also a good agreement with the CRMS (last column of the tables) for all moments except the Galactic *y*-direction component of the BF. In Figs 5 and 6 we show the bulk, shear and octupole flows as a function of the depth R_l for the COMPOSITE and SFI++ surveys. The error bars in Fig. 6 are for illustration and are the expected rms deviation, $\sqrt{\langle (U_i - u_i)^2 \rangle}$, of the estimated moment from the actual value of the ideal moment. Thus they represent a combination of measurement noise and deviation from the ideal window. We also show the expected CRMS of the flow as described above. As noted above, the BF is particularly sensitive

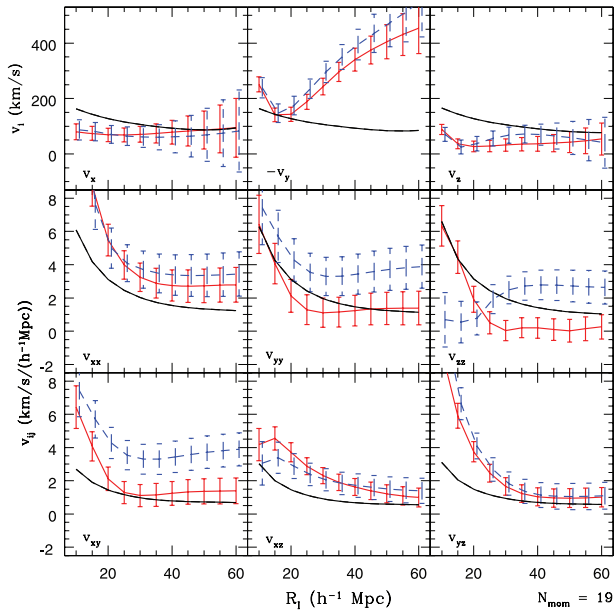


Figure 5. The BF and shear moments of the COMPOSITE (red solid line) and SFI++ (blue dashed line) catalogues as a function of R_l , all in Galactic coordinates. Note that the data points are not independent. The top panels are the BF velocities to the Galactic x - (left), y - (centre) and z - (left) directions. The error bars are as described in the text. In the middle and bottom panels, we show the shear components in the Galactic directions xx (middle left), yy (middle centre) and zz (middle right) and the xy (bottom left), yz (bottom centre) and zx (bottom right). The solid black line, without the error bars, in each panel is the *WMAP5* Λ CDM cosmic rms (CRMS).

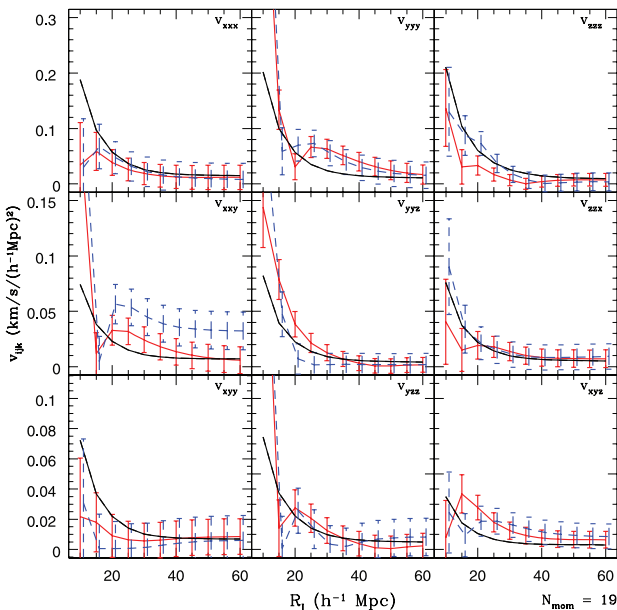


Figure 6. The same as Fig. 5 for the octupole moments. Galactic xxx (top left), yyy (top centre) and zzz (top right); xxy (middle left), yyz (middle centre) and zzx (middle right); the xyy (bottom left), yzz (bottom centre) and xyz (bottom right).

to the large scales of the matter power spectrum, and so the large amplitude of the BF is suggestive of excess power on scales $k \sim 0.01 \text{ h Mpc}^{-1}$.

4.2 Comparison with Λ CDM cosmology

To make the comparisons with cosmological models more precise, we compare, in a frequentist sense, the observed BF moments with the cosmological expectation. In other words, we calculate the probability that a randomly placed observer would have observed moments as large as the ones measured. Specifically, since each moment is Gaussian-distributed around zero mean, we calculate the χ^2 for N_{MOM} degrees of freedom corresponding to the number of moments, as given by

$$\chi^2 = \sum_{p=1}^{N_{\text{MOM}}} \sum_{q=1}^{N_{\text{MOM}}} u_p R_{pq}^{-1} u_q, \quad (27)$$

where p and q specify the BF, shear and octupole components of the covariance matrix R_{pq} for a specific set of values for the cosmological parameters we are interested in.

The results are presented in Table 4, where we show, for each of the catalogues, the per cent probability of getting a larger χ^2 , $P(> \chi^2)$. In the table, we break down the probabilities for $N_{\text{MOM}} = 3$ (BF alone), $N_{\text{MOM}} = 9$ (total, BF and shear) and for $N_{\text{MOM}} = 19$ into total, BF, shear and octupole. This has the benefit of showing us clearly which part of the flow is in agreement or disagreement with standard cosmology. Table 4 shows that although the BF is highly unlikely, both the shear and octupole moments amplitudes are more or less what is expected. For $N_{\text{MOM}} = 19$, the total probability of getting the observed χ^2 or higher is ~ 20 per cent, the probability of the shear alone is $\in [10, 50]$ per cent and the octupole ~ 80 per cent, whereas getting the BF is $\lesssim 0.5$ per cent.

Note that the BF is discrepant at the 99.78 and 97 per cent levels for the two independent subsamples (SFI++ and DEEP, respectively). Recall that the SFI++ peculiar velocities are based on the TF relation applied to field and group spirals, whereas the DEEP compilation is based on a variety of other methods, particularly SNIa and the FP relation in early-type galaxies. The agreement between these independent data sets indicates that the BF is not a result of systematic errors.

Thus when considered by itself, the BF disagrees with Λ CDM at $\gtrsim 98$ per cent CL, but there is no disagreement when all 19 moments are considered together. This is a consequence of the fact that we have only one component, the Galactic y -direction of the BF, that is much higher than expected. When considering only three components of the BF, then clearly if one disagrees, the χ^2 will be much higher (probability much lower) than if only one out of 19 amplitudes is in conflict. This trend is clearly shown in Table 4.

On the other hand, as noted above, for the shear and octupole moments, the measurement uncertainties are greater than for the BF because these moments are essentially derivatives of the (noisy) flow field. Thus the shear, for example, is not as powerful a cosmological probe as the BF, at least with current data sets. One way to quantify this is to compare the *WMAP5* CRMS to the measurement noise (see Figs 5, 6 and Tables 1, 2). In the case of the BF, this ratio is in the range 1.5–2.5, whereas for the shear it's 1–1.2 and for the octupole the values are only 0.5–1. Thus, while we have shown that these higher moments are not much different than expected, due to the noise we do not have much of a handle on their actual values. Consequently, the discriminatory power of these higher order moments (and their χ^2 values) is less than for the BF, since the

Table 4. The total observed $P(> \chi^2)$ in per cent for $N_{\text{MOM}} = 3, 9$ and 19 and for the BF, shear and octupole moments for each, for $R_l = 50 h^{-1}$ Mpc and the *WMAP5* central parameters $\Omega_m = 0.258$ $\sigma_8 = 0.796$.

	$N_{\text{MOM}} = 3$		$N_{\text{MOM}} = 9$		$N_{\text{MOM}} = 19$			
	BF	Total	BF	Shear	Total	BF	Shear	Octupole
COMPOSITE	1.89	6.01	1.81	41.76	17.00	0.50	52.60	78.33
SFI++	3.11	1.73	3.22	7.70	16.19	0.22	11.22	89.38
DEEP	6.02	30.41	6.29	82.62	55.54	3.18	91.22	81.61

contribution to the χ^2 from measurement-noise-dominated moments is always going to be about unity.

Finally, note that the shear tensor tabulated in Tables 1 and 2 and shown in Figs 5 has 6 components. In practice, however, the trace of the shear (i.e. the average expansion rate) is typically not measurable by peculiar velocity surveys, but is a free parameter that is usually adjusted to be close to zero by requiring that there be no net inflow or outflow of peculiar velocity tracers. Therefore, it is more conservative to consider the traceless components of the shear. If we subtract off one-third of the trace from each component on the diagonal (xx , yy and zz), we see that the measured shears are similar to the *WMAP5* expected rms values.

5 DISCUSSION

Our total BF, calculated for the COMPOSITE catalogue at $R_l = 50 h^{-1}$ Mpc, with $N_{\text{MOM}} = 19$ gives $|v| = 416 \pm 78 \text{ km s}^{-1}$ towards Galactic $l = 282^\circ \pm 11^\circ$ and $b = 6^\circ \pm 6^\circ$ which is in disagreement with the expectations of the *WMAP5* (Dunkley et al. 2009) cosmology at the 98–99.5 per cent CL. This result, however, is in excellent agreement with the results found previously (Paper I) estimating only the BF. The small magnitude of the shear and octupole moments suggest that our previous result was not due to, for example, aliased small-scale power contaminating the BF measurement. This shows that our orthogonality procedure (equation 7) works very well.

This BF value also agrees remarkably well with other peculiar velocity estimates (e.g. Hudson 1994; Hoffman et al. 2001; Zaroubi et al. 2001; Pike & Hudson 2005; Sarkar et al. 2007; Feldman & Watkins 2008; Lavaux et al. 2010), though these estimates were derived with different catalogues, methodologies and assumptions.

The results for the shear and octupole are consistent with the hypothesis that the power is not unusual on scales smaller than the very large ones probed by the BF. As mentioned above, another way to make such a comparison is via supercluster infall. For example, Pike & Hudson (2005) found $(\Omega_m/0.3)^{0.55} \sigma_8 = 0.80 \pm 0.05$, consistent with the mean *WMAP5*+BAO+SN values $(\Omega_m/0.3)^{0.55} \sigma_8 = 0.77 \pm 0.035$ (Komatsu et al. 2009). Abate & Erdoğdu (2009), who studied the velocity correlation function of SFI++, a statistic that mixes a range of scales, also found consistency with *WMAP5* cosmological parameters. Thus it does seem to be the BF which is unusual.

Recently, Kashlinsky et al. (2008, 2010) and Atrio-Barandela et al. (2010) claimed to have detected a dipole in filtered *WMAP* CMB temperature maps measured at the locations of rich clusters. The magnitude of this cluster–temperature dipole is $2.8 \pm 0.7 \text{ K}$. The authors interpret this as being due to the kinetic Sunyaev–Zel’dovich (kSZ) effect, implying a large-scale flow with a bulk velocity in the range $\in [600, 1000] \text{ km s}^{-1}$ towards $l = 283^\circ \pm 14^\circ$, $b = 12^\circ \pm 14^\circ$. Although the scale of their cluster catalogues ($z \sim 0.1\text{--}0.2$) is of order three or more times the scales that our catalogues probe,

this kSZ flow is in excellent directional agreement with the one we detected here and in Paper I. The magnitude is larger, but the authors caution that the magnitude is systematically uncertain. We note that the BF that we detect does not seem to level-off yet and there is no clear sign of convergence to the CMB frame in our catalogues (see Fig. 5, top centre panel). We by no means claim to verify the Kashlinsky et al. (2008, 2010) results, however, we certainly cannot refute it with our data.

The motion we detect is not due to nearby sources, such as the Great Attractor (distance of $\sim 40 h^{-1}$ Mpc), but rather to sources at greater depths that have yet to be fully identified. The largest known mass concentration, the Shapley supercluster, does not seem to be massive enough to cause a flow of this magnitude (Raychaudhury 1989). It is likely that the flow arises both from various mass concentrations in the Galactic y -direction as well as underdense regions in the opposite direction. Currently, there is no peculiar velocity survey in existence that is deep enough to resolve the source(s) of the flow, if indeed it is a potential flow.

A good measure for the distance scale to the sources responsible for most of the BF is the ratio of the BF to shear (Lilje et al. 1986; Kaiser 1991). This characteristic depth $D_i \propto u_i/u_{ii}$ with constant of proportionality of order one should be valid even if multiple sources, including underdense regions, as expected for a Gaussian random field, are responsible for the flow. In Fig. 7, we show the

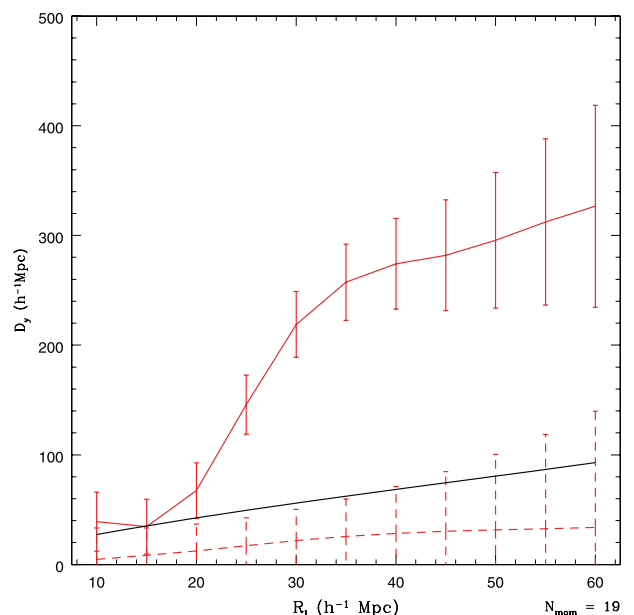


Figure 7. The expected distance to the dominant gravitational sources (solid line) (u_y/u_{yy}) as a function of R_l for the COMPOSITE survey as well as an expected distance using the *WMAP5* central parameters (solid line, no error bars) discussed in the paper. For comparison we also show u_x/u_{xx} (dashed line) that agrees with the *WMAP5* expectations within errors.

effective distance $D_y \propto u_y/u_{yy}$ to an attractor for the COMPOSITE survey as a function of R_l . Nearby, where $R_l \lesssim 30 h^{-1}$ Mpc, the moments are dominated by the nearby velocity field and show the effect of the Great Attractor at $\sim 35 h^{-1}$ Mpc. Then there is a sudden rise around $30 h^{-1}$ Mpc that suggests that on scales beyond the Great Attractor, the flow is driven by even larger and more distant mass concentration(s) in the same general direction. The uncertainties are large, however, at $R_l = 50 h^{-1}$ Mpc; we find a characteristic distance of $296 \pm 62 h^{-1}$ Mpc, much larger than the expected *WMAP5* value of $82 h^{-1}$ Mpc. For comparison, we show the estimated u_x/u_{xx} which is consistent with the *WMAP5* expected results.

Note, however, as discussed above, it is sensible to subtract one-third of the trace of the shear tensor from each diagonal component. In this case, the yy component of the shear tensor is consistent with zero, implying that the attractor is at infinity. Thus, we cannot exclude the coherent flow on much larger scales claimed by Kashlinsky et al. (2008, 2010).

6 CONCLUSIONS

We have estimated the MV BF, shear and octupole moments and showed that they are minimally sensitive to aliasing from small-scale power. We have applied the MV formalism to a number of compilations of recent peculiar velocity surveys. The MV WFs are similar to the ideal WFs and our octupole moments orthogonalization procedure works well in a sense that including them does not affect the BF much.

The various peculiar velocity surveys are consistent with each other and all show a large BF which does not follow expectations from the *WMAP5*-normalized Λ CDM model. Specifically, we have shown that the BF within a Gaussian window of radius $R_l = 50 h^{-1}$ Mpc has a magnitude of $416 \pm 78 \text{ km s}^{-1}$ towards Galactic $l = 282^\circ \pm 11^\circ$ and $b = 6^\circ \pm 6^\circ$ in disagreement with *WMAP5* (Dunkley et al. 2009) at the 99.5 per cent CL. This flow is consistent with being relatively ‘cold’ (both shear and octupole moments are in agreement with expectations) and is not due to nearby sources. If we include all 19 octupole (nine shear) moments, we disagree with the *WMAP5* expectations at only the 83 per cent (94 per cent) CL, respectively. We also found that the sources responsible for the BF are at an effective distance of $> 300 h^{-1}$ Mpc, too far to identify in existing all-sky redshifts surveys.

If the flow is a potential flow, there are various possible explanations as to its source. While it is always possible that the result is due to systematic errors in the data, we tend to discount this possibility since the BF is seen in many independent surveys with various distance indicators, methodologies and geometries. It may be that we live in a Λ CDM Universe but that we happen to live in one of the very rare volumes that exhibits this flow ($\lesssim 1$ per cent), or we may live in a Universe with more large-scale power than *WMAP5*-normalized Λ CDM. In either of these last two cases, we may be able to find the source or sources of the flow in future redshift surveys. It is of course likely that the sources are a combination of overdense and underdense regions and not just a single large mass concentration.

ACKNOWLEDGMENTS

We thank our referee, Michael Strauss, for useful comments. HAF has been supported in part by an NSF grant AST-0807326, by a grant from the Research Corporation, by the National Science Foundation through TeraGrid resources provided by the NCSA, by the University of Kansas General Research Fund (KUGRF) and acknowledges

the hospitality of University College, London and Imperial College in the UK and the Institut d’Astrophysique de Paris, France. MJH has been supported by NSERC and acknowledges the hospitality of the Institut d’Astrophysique de Paris, and the financial support of the IAP/UPMC visiting programme and the French ANR (OTARIE).

REFERENCES

- Abate A., Erdoğan P., 2009, *MNRAS*, 400, 1541
Atrio-Barandela F., Kashlinsky A., Ebeling H., Kocevski D., Edge A., 2010, *ApJ*, in press
Bardeen J. M., Bond J. R., Kaiser N., Szalay A. S., 1986, *ApJ*, 304, 15
Bernardi M., Alonso M. V., da Costa L. N., Willmer C. N. A., Wegner G., Pellegrini P. S., Rité C., Maia M. A. G., 2002, *AJ*, 123, 2990
Cole S. et al., 2005, *MNRAS*, 362, 505
Colless M., Saglia R. P., Burstein D., Davies R. L., McMahan R. K., Wegner G., 2001, *MNRAS*, 321, 277
da Costa L. N., Bernardi M., Alonso M. V., Wegner G., Willmer C. N. A., Pellegrini P. S., Rité C., Maia M. A. G., 2000, *AJ*, 120, 95
Dale D. A., Giovanelli R., Haynes M. P., Campusano L. E., Hardy E., 1999a, *AJ*, 118, 1489
Dunkley J. et al., 2009, *ApJS*, 180, 306
Eisenstein D. J., Hu W., 1998, *ApJ*, 496, 605
Eisenstein D. J. et al., 2005, *ApJ*, 633, 560
Feldman H. A., Watkins R., 2008, *MNRAS*, 387, 825
Feldman H. A., Frieman J. A., Fry J. N., Scoccimarro R., 2001, *Phys. Rev. Lett.*, 86, 1434
Feldman H. A. et al., 2003, *ApJ*, 596, L131
Fu L. et al., 2008, *A&A*, 479, 9
Giovanelli R., Haynes M. P., Salzer J. J., Wegner G., da Costa L. N., Freudling W., 1998b, *AJ*, 116, 2632
Ho S., Hirata C. M., Padmanabhan N., Seljak U., Bahcall N., 2008, *Phys. Rev. D*, 78, 043519
Hoffman Y., Eldar A., Zaroubi S., Dekel A., 2001, *ApJ*, submitted (astro-ph/0102190)
Hudson M. J., 1994, *MNRAS*, 266, 475
Hudson M. J., Smith R. J., Lucey J. R., Schlegel D. J., Davies R. L., 1999, *ApJ*, 512, L79
Hudson M. J., Smith R. J., Lucey J. R., Branchini E., 2004, *MNRAS*, 352, 61
Jaffe A. H., Kaiser N., 1995, *ApJ*, 455, 26
Juszkiewicz R., Feldman H. A., Fry J. N., Jaffe A. H., 2010, *J. Cosmol. Astropart. Phys.*, 2, 21
Kaiser N., 1988, *MNRAS*, 231, 149
Kaiser N., 1991, *ApJ*, 366, 388
Kashlinsky A., Atrio-Barandela F., Kocevski D., Ebeling H., 2008, *ApJ*, 686, L49
Kashlinsky A., Atrio-Barandela F., Ebeling H., Edge A., Kocevski D., 2010, *ApJ*, 712, L81
Komatsu E. et al., 2009, *ApJS*, 180, 330
Lauer T. R., Postman M., 1994, *ApJ*, 425, 418 (LP)
Lavaux G., Tully R. B., Mohayaee R., Colombi S., 2010, *ApJ*, 709, 483
Lilje P. B., Yahil A., Jones B. J. T., 1986, *ApJ*, 307, 91
Masters K. L., Springob C. M., Haynes M. P., Giovanelli R., 2006, *ApJ*, 653, 861
Neill J. D., Hudson M. J., Conley A., 2007, *ApJ*, 661, L123
Park C.-G., Park C., 2006, *ApJ*, 637, 1
Peacock J. A. et al., 2001, *Nat*, 410, 169
Percival W. J., Cole S., Eisenstein D. J., Nichol R. C., Peacock J. A., Pope A. C., Szalay A. S., 2007, *MNRAS*, 381, 1053
Pike R. W., Hudson M. J., 2005, *ApJ*, 635, 11
Radburn-Smith D. J., Lucey J. R., Hudson M. J., 2004, *MNRAS*, 355, 1378
Raychaudhury S., 1989, *Nat*, 342, 251
Sachs R. K., Wolfe A. M., 1967, *ApJ*, 147, 73
Sarkar D., Feldman H. A., Watkins R., 2007, *MNRAS*, 375, 69
Scoccimarro R., Feldman H. A., Fry J., Frieman J. A., 2001, *ApJ*, 546, 652

- Springob C. M., Masters K. L., Haynes M. P., Giovanelli R., Marinoni C., 2007, *ApJS*, 172, 599
- Springob C. M., Masters K. L., Haynes M. P., Giovanelli R., Marinoni C., 2009, *ApJS*, 182, 474
- Strauss M. A., Willick J. A., 1995, *Phys. Rep.*, 261, 271
- Tegmark M. et al., 2004, *ApJ*, 606, 702
- Tonry J. L., Dressler A., Blakeslee J. P., Ajhar E. A., Fletcher A. B., Luppino G. A., Metzger M. R., Moore C. B., 2001, *ApJ*, 546, 681
- Tonry J. L. et al., 2003, *ApJ*, 594, 1
- Verde L. et al., 2002, *MNRAS*, 335, 432
- Watkins R., Feldman H. A., 2007, *MNRAS*, 379, 343
- Watkins R., Feldman H. A., Hudson M. J., 2009, *MNRAS*, 392, 743 (Paper I)
- Wegner G. et al., 2003, *AJ*, 126, 2268
- Willick J. A., 1999, *ApJ*, 522, 647
- Zaroubi S., Bernardi M., da Costa L. N., Hoffman Y., Alonso M. V., Wegner G., Willmer C. N. A., Pellegrini P. S., 2001, *MNRAS*, 326, 375

This paper has been typeset from a \TeX/L\AA\TeX file prepared by the author.